Disordered carbon nanotube alloys in the effective-medium supercell approximation

Rostam Moradian*
Physics Department, Faculty of Science, Razi University, Kermanshah, Iran
and Computational Physical Science Research Laboratory, Department of Nano-Science, Institute for Studies in Theoretical Physics and Mathematics (IPM), P.O.Box 19395-1795, Tehran, Iran

(Received 19 August 2004; published 23 November 2004; corrected 8 December 2004)

We investigate a disordered single-walled carbon nanotube (SWCNT) in an effective-medium supercell approximation (EMSCA). The first type of disorder that we consider is the presence of vacancies. Our results show that the vacancies induce some bound states on their neighbor host sites, leading to the creation of a band around the Fermi energy in the SWCNT average density of states. The second type of disorder considered is a substitutional $B_{cb}N_{cn}C_{1-cb-cn}$ alloy due to its applications in hetrojunctions. We found that for a fixed boron (nitrogen) concentration, by increasing the nitrogen (boron) concentration the averaged semiconducting gap E_g decreases and disappears at a critical concentration. A consequence of our results for nanoelectronic devices is that by changing the boron (nitrogen) concentration, one can make a semiconductor SWCNT with a predetermined energy gap.

DOI: 10.1103/PhysRevB.70.205425 PACS number(s): 61.46.+w, 71.55.Ak, 73.63.−b, 74.70.Ad

I. INTRODUCTION

The role of disorder in a single-walled carbon nanotube (SWCNT) is of importance from two prospectives; first in the growth process of a SWCNT due to the experimental environment some impurity atoms are inserted and vacancies are created.[1–3] Second, we deliberately implant the impurity so as to construct nanotube alloys, such as $B_{cb}C_{1-cb}$, $N_{cn}C_{1-cn}$ and $B_{cb}N_{cn}C_{1-cb-cn}$ SWCNTs,[4–7] with predetermined physical properties. In the first case, the effect of a point-like defect was investigated by calculation of electron reflection coefficient,[8] and also two substitute defects in an armchair SWCNT.[9] It has been found that the symmetry of defects strongly affected the conductance and the local density of states. By different techniques, the boron nitride SWCNTs junctions,[10,11] the spin polarization in a quasi-one-dimensional C/BN nanotube,[12] and also the current distribution in boron and nitrogen doped SWCNTs were investigated.[13] For finite impurity concentration, a systematic field theory technique beyond single-site T-matrix approximation has not yet been applied to the disordered SWCNTs.[14] In this paper, by applying the effective-medium supercell approximation (EMSCA)[15,16] method to the disordered SWCNT, we will go beyond this approximation and consider the presence of finite impurities. We provide a more realistic description of the effects of disorder, due to vacancies, on an armchair SWCNT's and a zigzag SWCNT's density of states (dos). Also in this formalism, we address the question of how the doping of a zigzag SWCNT by boron (nitrogen), i.e., $B_{cb}N_{cn}C_{1-cb-cn}$, controls the semiconducting gap E_g.

II. MODEL AND FORMALISM

Let us consider the Hamiltonian as a general random tight-binding model[15]

$$H = -\sum_{ij\alpha\beta\sigma} t_{ij}^{\alpha\beta} c_{i\sigma}^{\alpha\dagger} c_{j\sigma}^{\beta} + \sum_{i\alpha\sigma} (\varepsilon_i^{\alpha} - \mu)\hat{n}_{i\sigma}^{\alpha}, \qquad (1)$$

where α and β refer to the A or B sites inside of the graphene Bravais lattice unit cell, where each Bravais lattice site includes two nonequivalent sites that are indicated by A and B, $c_{i\sigma}^{\alpha\dagger}$ ($c_{i\sigma}^{\alpha}$) is the creation (annihilation) operator of an electron with spin σ on Bravais lattice site i, and $\hat{n}_{i\sigma}^{\alpha} = c_{i\sigma}^{\alpha\dagger} c_{i\sigma}^{\alpha}$ is the number operator. $t_{ij\sigma\sigma}^{\alpha\beta}$ are the hopping integrals between the π orbitals of sites i and j with spin σ. μ is the chemical potential and ε_i^{α} is the random on-site energy where it takes 0 with probability $1-c$ for host sites and δ with probability c for impurity sites. For the $B_{cb}N_{cn}C_{1-cb-cn}$ SWCNT alloy, ε_i^{α} takes $\varepsilon_b^{\alpha} = 2.33$ eV with probability cb for boron sites, $\varepsilon_n^{\alpha} = -2.50$ eV with probability cn for nitrogen sites and $\varepsilon_c^{\alpha} = 0$ eV with probability $1-cb-cn$ for the carbon sites, if measured with respect to ε_c^{α}.[6,7] Figure 1 shows a two-dimensional graphene sheet. Each cell of the Bravias lattice includes two nonequivalent sites that are denoted by A and B. The primitive vectors of the Bravias lattice are $\mathbf{a}_1$ and $\mathbf{a}_2$ and the chiral vector is $\mathbf{L}$. The heavy dashed line on the figure shows a four-site supercell of the graphene Bravias lattice.

The SWCNT can be construct by role up a two-dimension graphene sheet in some specified directions with the periodic boundary condition along the circumference direction.[17] Following this, rolling up chiral vector $\mathbf{L}$ has been fixed on the x axes of the two-dimensional (2D) graphene sheet, hence

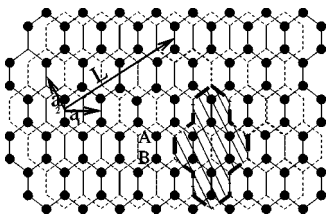

FIG. 1. A two-dimensional graphene sheet. The light dashed lines illustrate the Bravais lattice unit cells, $\mathbf{a}_1$ and $\mathbf{a}_2$ are the primitive vectors. Each cell includes two nonequivalent sites, which are denoted by A and B. $L = n_1\mathbf{a}_1 + n_2\mathbf{a}_2$ is the chiral vector. For an armchair SWCNT $n_1 = n$ and $n_2 = 2n$, while for a zigzag SWCNT $n_1 = n$ and $n_2 = 0$. The heavy dashed line denotes a four-site supercell.

the carbon nanotube axes is coincident on the *y* axes. Therefore the real lattice primitive vectors $\mathbf{a}_1$ and $\mathbf{a}_2$ and their corresponding reciprocal lattice primitive vectors $\mathbf{b}_1$ and $\mathbf{b}_2$ for a zigzag SWCNT are

$$\mathbf{a}_1 = a\mathbf{i}, \quad \mathbf{a}_2 = \frac{a}{2}(-\mathbf{i} + \sqrt{3}\mathbf{j}),$$

$$\mathbf{b}_1 = \frac{2\pi}{a}\left(\mathbf{i} + \frac{\mathbf{j}}{\sqrt{3}}\right), \quad \mathbf{b}_2 = \frac{2\mathbf{j}}{\sqrt{3}}\frac{2\pi}{a}, \tag{2}$$

and for an armchair are given by

$$\mathbf{a}_1 = a\mathbf{j}, \quad \mathbf{a}_2 = \frac{a}{2}(-\mathbf{j} + \sqrt{3}\mathbf{i}),$$

$$\mathbf{b}_1 = \frac{2\pi}{a}\left(\frac{\mathbf{i}}{\sqrt{3}} + \mathbf{j}\right), \quad \mathbf{b}_2 = \frac{2\mathbf{i}}{\sqrt{3}}\frac{2\pi}{a}, \tag{3}$$

where $\mathbf{i}$ and $\mathbf{j}$ are the unit vectors of the *x*-*y* graphene plane and $a = |\mathbf{a}_1|$. The periodic boundary condition in the *x* direction imply that

$$\exp(\imath k_x L) = 1, \tag{4}$$

where *L* is the length of the chiral vector, $L = |\mathbf{L}|$. For a zigzag SWCNT $L = na$ and for an armchair is $L = \sqrt{3}na$. So the periodicity condition Eq. (4) implies that the *x* component of the wave-vectors k_x is restricted to

$$k_x = \frac{2\pi m}{L}, \tag{5}$$

where *m* is an integer number.

The matrix form of Eq. (1) is

$$H = -\sum_{ij\sigma} \Psi^{\dagger}_{i\sigma} \hat{t}_{ij} \Psi_{j\sigma} + \sum_{i\sigma} \Psi^{\dagger}_{i\sigma}(\hat{\varepsilon}_i - \mu\mathbf{I})\Psi_{i\sigma}, \tag{6}$$

where the two-component field operator, $\Psi^{\dagger}_{i\sigma}$, is given by

$$\Psi_{i\sigma} = \begin{pmatrix} c^{\mathrm{A}}_{i\sigma} \\ c^{\mathrm{B}}_{i\sigma} \end{pmatrix}, \tag{7}$$

and $\hat{\varepsilon}_i$ is the random on-site energy matrix

$$\hat{\varepsilon}_i = \begin{pmatrix} \varepsilon^{\mathrm{A}}_i & 0 \\ 0 & \varepsilon^{\mathrm{B}}_i \end{pmatrix}, \tag{8}$$

and $\hat{t}_{ij}$ is the hopping matrix defined by

$$\hat{t}_{ij} = \begin{pmatrix} t^{\mathrm{AA}}_{ij} & t^{\mathrm{AB}}_{ij} \\ t^{\mathrm{BA}}_{ij} & t^{\mathrm{BB}}_{ij} \end{pmatrix}, \tag{9}$$

and $\mathbf{I}$ is a 2×2 unitary matrix.

The equation of motion for electrons in such a lattice is,

$$\sum_l \left[(E\mathbf{I} - \hat{\varepsilon}_i + \hat{\mu}_i)\delta_{il} - \hat{t}_{il}\right]\mathbf{G}(l,j;E) = \mathbf{I}\delta_{ij}, \tag{10}$$

where $\mathbf{G}(i,j;E)$ is the random Green function matrix defined by

$$\mathbf{G}(i,j;E) = \begin{pmatrix} G^{\mathrm{AA}}(i,j;E) & G^{\mathrm{AB}}(i,j;E) \\ G^{\mathrm{BA}}(i,j;E) & G^{\mathrm{BB}}(i,j;E) \end{pmatrix}. \tag{11}$$

We considered the $\hat{\varepsilon}_i$ as a perturbation parameter, hence $\mathbf{G}(i,j;E)$ in Eq. (10), may be expanded in terms of the perfect Green's, function matrix $\mathbf{G}^0(i,j;E)$ as

$$\mathbf{G}(i,j;E) = \mathbf{G}^0(i,j;E) + \sum_l \mathbf{G}^0(i,l;E)\hat{\varepsilon}_l \mathbf{G}(l,j;E), \tag{12}$$

where $\mathbf{G}^0(i,j;E)$ is given by

$$\mathbf{G}^0(i,j;E) = \frac{2}{N}\sum_{\mathbf{k}} e^{\imath \mathbf{k}.\mathbf{r}_{ij}}\left(E\mathbf{I} - \hat{\varepsilon}_{\mathbf{k}} + \mathbf{I}\mu\right)^{-1}, \tag{13}$$

with $\hat{\epsilon}_{\mathbf{k}} = \frac{2}{N}\Sigma_{ij}\hat{t}_{ij}e^{\imath \mathbf{k}.\mathbf{r}_{ij}}$ being the band structure for perfect system. In our calculations we take $\mu = 0$, the hopping randomness are neglected also we assumed allowed hopping to the nearest neighbors and neglected the others,

$$t^{\mathrm{AB}}_{\langle ij\rangle} = t^{\mathrm{BA}}_{\langle ij\rangle} = t, \tag{14}$$

where $t \sim 3$ eV is clean system nearest-neighbour hopping integral. Hence

$$\hat{t}_{\langle ij\rangle} = \begin{pmatrix} 0 & t^{\mathrm{AB}}_{\langle ij\rangle} \\ t^{\mathrm{BA}}_{\langle ij\rangle} & 0 \end{pmatrix}, \tag{15}$$

and the dispersion relation is

$$\hat{\varepsilon}_{\mathbf{k}} = \begin{pmatrix} 0 & t\gamma(\mathbf{k}) \\ t\gamma^*(\mathbf{k}) & 0 \end{pmatrix}, \tag{16}$$

where $\gamma(\mathbf{k}) = \Sigma_{i=1}^{3} e^{\imath \mathbf{k}.\tau_i}$ and τ_i are three vectors that connect an A (B) site to its nearest neighbors B(A) sites.

The Dyson equation for the averaged Green function, $\overline{\mathbf{G}}(i,j;E)$, corresponding to Eq. (12) is

$$\overline{\mathbf{G}}(i,j;E) = \mathbf{G}^0(i,j;E) + \sum_{ll'} \mathbf{G}^0(i,l;E)\boldsymbol{\Sigma}(l,l';E)\overline{\mathbf{G}}(l',j;E), \tag{17}$$

where the self energy $\boldsymbol{\Sigma}(l,l';E)$ is defined by

$$\langle \hat{\varepsilon}_l \mathbf{G}(l,j;E)\rangle = \sum_{l'} \boldsymbol{\Sigma}(l,l';E)\overline{\mathbf{G}}(l',j;E). \tag{18}$$

The Fourier transform of $\overline{\mathbf{G}}(i,j;E)$ in Eq. (17) is given by

$$\overline{\mathbf{G}}(i,j;E) = \frac{2}{N}\sum_{\mathbf{k}} e^{\imath \mathbf{k}.\mathbf{r}_{ij}}(E\mathbf{I} - \hat{\varepsilon}_{\mathbf{k}} + \mu\mathbf{I} - \boldsymbol{\Sigma}(\mathbf{k};E))^{-1}, \tag{19}$$

where

$$\boldsymbol{\Sigma}(\mathbf{k};E) = \frac{2}{N}\sum_{i,j} e^{-\imath \mathbf{k}.\mathbf{r}_{ij}}\boldsymbol{\Sigma}(i,j;E), \tag{20}$$

is the self-energy Fourier transform. Since Eqs. (19) and (17) could not be solved exactly, different single site approximations such as Born approximation, coherent potential approximation, etc.,[14] have been applied to solve these equations. Here by using EMSCA we are going beyond such single site approximations.

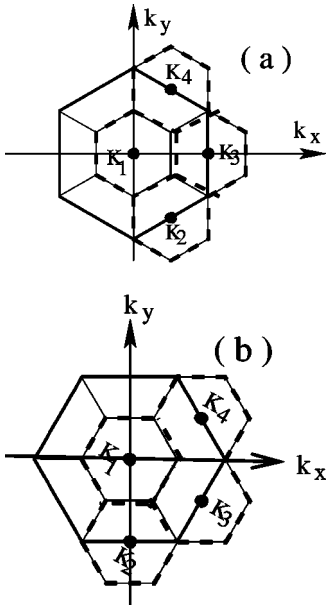

FIG. 2. First Brillouin zone and the patches of supercell wave vectors $\mathbf{K}_n$ where they are corresponding to a four-sites supercell in real space for: (a) an armchair SWCNT where the supercell wave vectors are $\mathbf{K}_1=0$, $\mathbf{K}_2=(-\mathbf{b}_1+\mathbf{b}_2)/2$, $\mathbf{K}_3=\mathbf{b}_2/2$, $\mathbf{K}_4=\mathbf{b}_1/2$, and (b) a zigzag SWCNT where the supercell wave vectors are $\mathbf{K}_1=0$, $\mathbf{K}_2=-\mathbf{b}_2/2$, $\mathbf{K}_3=(\mathbf{b}_1-\mathbf{b}_2)/2$, and $\mathbf{K}_4=\mathbf{b}_1/2$. The heavy lines indicate the FBZ and the dashed lines illustrate the patches where belong to each $\mathbf{K}_n$.

III. EFFECTIVE MEDIUM SUPER CELL APPROXIMATION (EMSCA) TREATMENT

We solve Eq. (12) using the EMSCA method[15,16] for the case of four sites supercell, i.e., $N_c=4$.

In the EMSCA technique, the supercell random Green's functions, $\mathbf{G}_{\rm sc}^{\rm im}(i,j;E)$, are related to the cavity Green's function $\hat{\mathcal{G}}(i,j;E)$ via[16]

$$\mathbf{G}_{\rm sc}^{\rm im}(I,J;E)=\hat{\mathcal{G}}(I,J;E)+\sum_{L}\hat{\mathcal{G}}(I,L;E)\hat{\varepsilon}_L\mathbf{G}_{\rm sc}^{\rm im}(L',J;E), \tag{21}$$

where $\{I\}$ refers to the sites inside the supercell. Also the Dyson's-like equation for the average supercell Green's function $\overline{\mathbf{G}}_{\rm sc}(I,J;E)$ is given by

$$\overline{\mathbf{G}}_{\rm sc}(I,J;E)=\hat{\mathcal{G}}(I,J;E)+\sum_{LL'}\hat{G}_{sc}(I,L;E)\mathbf{\Sigma}_{\rm sc}(L,L';E)\mathbf{G}(L',J;E). \tag{22}$$

The Fourier transform of $\overline{\mathbf{G}}_{\rm sc}(I,J;E)$ in Eq. (22) to the supercell wave vectors $\{\mathbf{K}_n\}$ is

$$\overline{\mathbf{G}}_{\rm sc}(\mathbf{K}_n;E)=\hat{\mathcal{G}}(\mathbf{K}_n;E)+\hat{\mathcal{G}}(\mathbf{K}_n;E)\mathbf{\Sigma}_{\rm sc}(\mathbf{K}_n;E)\mathbf{G}(\mathbf{K}_n;E), \tag{23}$$

where

$$\mathbf{\Sigma}(\mathbf{K}_n;E)=\frac{1}{N_c}\sum_{IJ}e^{\mathbf{K}_n\cdot\mathbf{r}_{IJ}}\mathbf{\Sigma}_{\rm sc}(I,J;E) \tag{24}$$

and

$$\overline{G}(\mathbf{K}_n;E)=\frac{N_c}{N}\sum_{\mathbf{k}\in\text{nth patches}}(\mathbf{I}E-\hat{\varepsilon}_{\mathbf{k}}+\mathbf{I}\mu-\mathbf{\Sigma}(\mathbf{K}_n;E))^{-1}. \tag{25}$$

The supercell wave vector $\{\mathbf{K}_n\}$ is defined by[15,16]

$$\mathbf{K}_n=\sum_{i=1}^{3}\frac{l_i}{N_{ci}}\mathbf{b}_i, \tag{26}$$

where N_{ci} are the number of Bravias lattice sites inside of the supercell in the ith direction and $\{\mathbf{b}_i\}$ are the reciprocal lattice primitive vectors and l_i is an integer number.

For a four-site supercell ($Nc=4$) SWCNT, where $Nc_1=2$ and $Nc_2=2$, Eq. (26) is reduced to

$$\{\mathbf{K}_n\}=\left\{\frac{l_1}{2}\mathbf{b}_1+\frac{l_2}{2}\mathbf{b}_2\right\}. \tag{27}$$

Therefore for zigzag SWCNT's Eq. (27) is convert to,

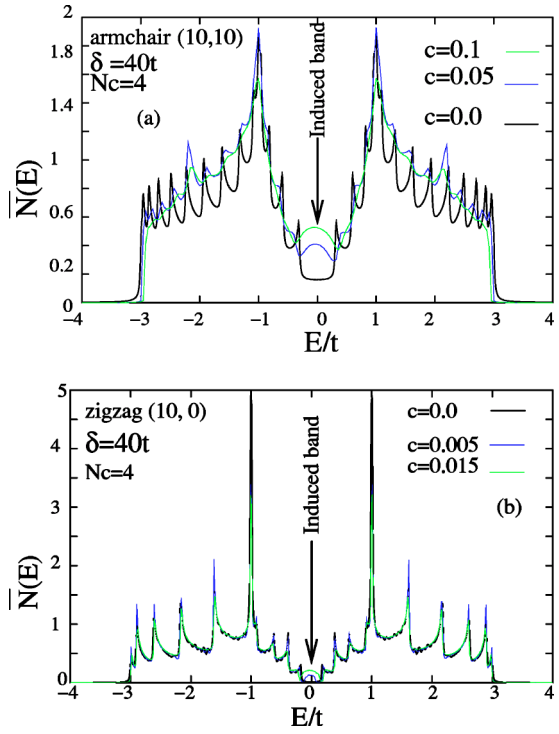

FIG. 3. (a) Comparison of average density of states for a (10,10) armchair SWCNT and (b) for a (10,0) zigzag SWCNT at $\delta=40t$ and different impurity concentration. At high random energies, $\delta \gg$ bandwidth, we have band splitting and the impurity band is located at higher energies, while remaining sites are the vacancies that induce a band around the Fermi energy. By increasing the vacancy concentration, the height of the peak at the Fermi energy increases and the van Hove singularities are smeared out.

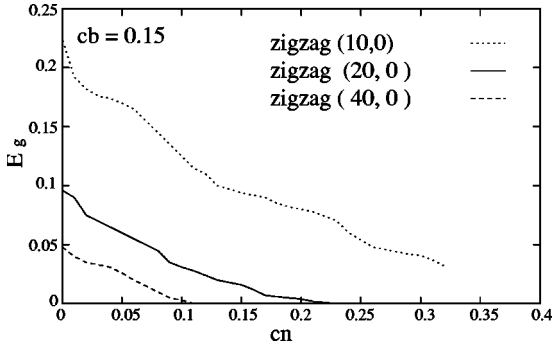

FIG. 4. The figure shows the effects of nitrogen doping on semiconducting gap E_g for a (10,0), (20,0), and (40,0) zigzag SWCNT alloy.

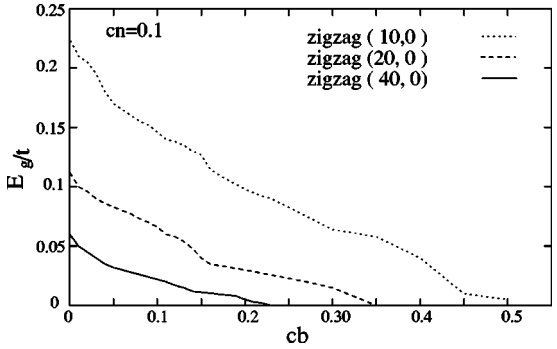

FIG. 6. Figure shows the effects of boron doping on the semiconducting gap E_g in a (10,0), (20,0), and (40,0) zigzag SWCNT alloy.

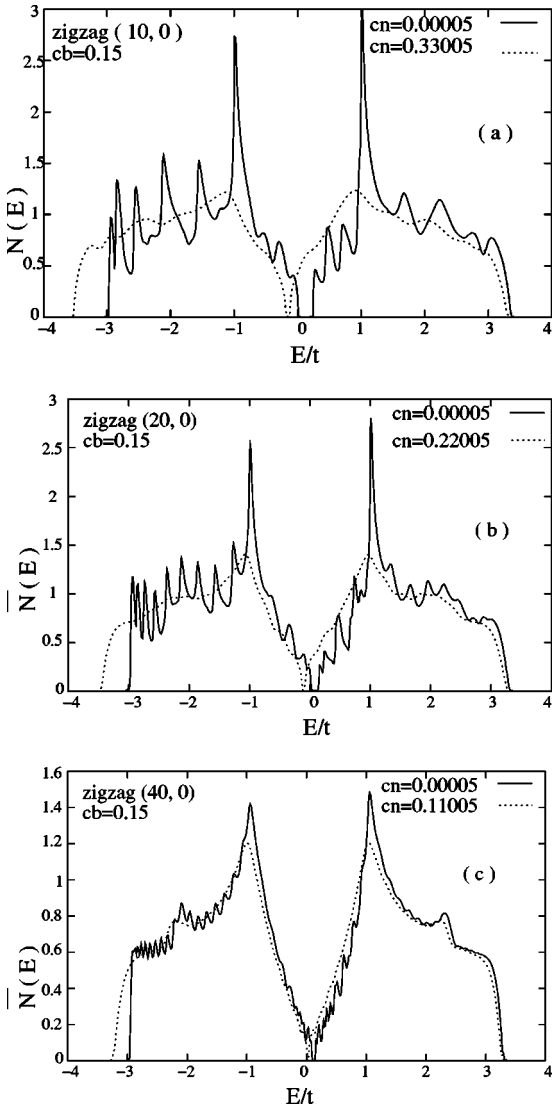

FIG. 5. The effects of nitrogen doping on a (10,0), (20,0), and (40,0) zigzag SWCNT's average density of states. At a fixed boron concentration $cb=0.15$, the average density of states for two nitrogen concentrations, low $cn=0.0005$ and high, are compared. For (20,0) and (40,0), at the critical concentration E_g is zero and the van Hove singularities disappear.

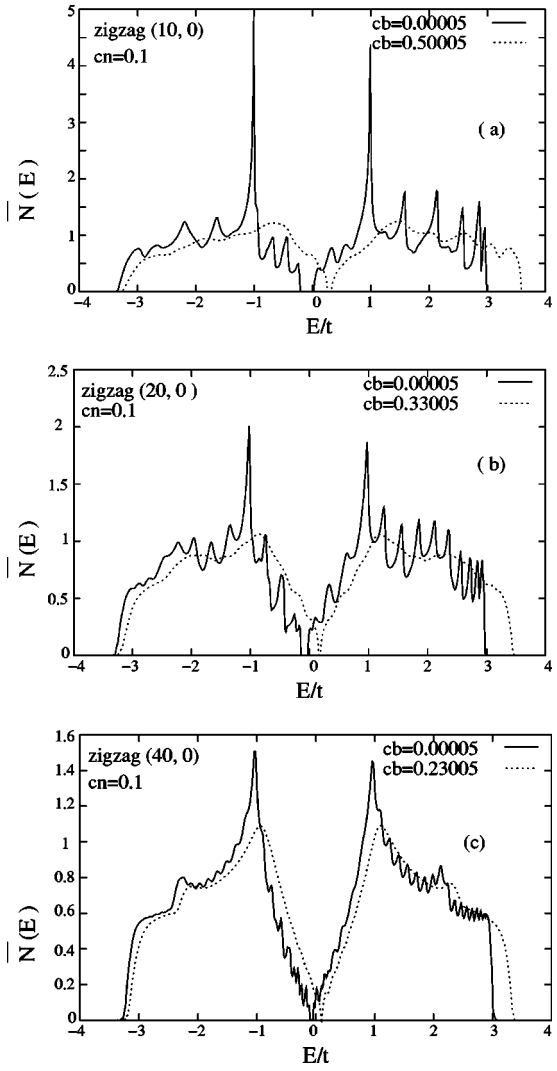

FIG. 7. Effects of boron doping on a (10,0), (20,0), and (40,0) zigzag SWCNT's average density of states. At a fixed nitrogen concentration of $cn=0.1$, the average density of states for two boron concentrations are compared. For (20,0), (40,0) at a critical concentration, E_g is closed and the van Hove singularities disappears and a semiconductor semimetal phase transition takes place.

$$\mathbf{K}_1 = 0;\ \mathbf{K}_2 = -\frac{\mathbf{b}_2}{2};\ \mathbf{K}_3 = \frac{\mathbf{b}_1 - \mathbf{b}_2}{2};\ \mathbf{K}_4 = \frac{\mathbf{b}_1}{2} \quad (28)$$

and for an armchair SWCNT are,

$$\mathbf{K}_1 = 0;\quad \mathbf{K}_2 = \frac{-\mathbf{b}_1 + \mathbf{b}_2}{2};\quad \mathbf{K}_3 = \frac{\mathbf{b}_2}{2};\quad \mathbf{K}_4 = \frac{\mathbf{b}_1}{2}. \quad (29)$$

Figures 2 illustrate the location of the supercell wavevectors $\{\mathbf{K}_n\}$ in the Brillouin zone corresponding to Eqs. (28) and (29) for a zigzag and an armchair SWCNT, respectively.

To calculate the $\overline{G_{sc}}(I,J;E)$ and $G_{sc}^{im}(I,J;E)$, Eqs. (21)–(25) should be solved self-consistently.

IV. RESULTS AND DISCUSSION

A SWCNT with vacancies is considered, the averaged density of states for different vacancy concentrations is calculated. We found that vacancies create some bound states around the Fermi level on their host neighbor sites, hence constructing a band in the averaged density of states. Also the one-dimensional (1D) van Hove singularities in high vacancy concentrations disappear. Figures 3(a) and 3(b) show the comparison between the average density of states for different vacancy concentrations in (10, 10) and (10, 0) SWCNTs, respectively. The bound states due to vacancies around the Fermi energy is marked by an arrow. In short, our results show that vacancies not only change the average density of states but also the number of electrons located on the host sites and also at high vacancy concentrations SWCNT's loses their 1D characteristics and become similar to a 2D disordered geraphene sheet.

We now investigate the effect of nitrogen and boron doping on a (10,0), (20,0), and (40,0) zigzag SWCNT. Two cases are considered, first fixed boron concentration at $cb=0.15$, with variable nitrogen concentration. In this case, we found that the average semiconducting gap, E_g, decreased by increasing the nitrogen concentration, and in some of them, (20,0) and (40,0), at a critical concentration disappeared. Figure 4 illustrates the effects of the nitrogen doping on the E_g. To clarify our results, we compare the average density of states for low and high nitrogen concentrations. Figure 5 compares the average density of states for the low, $cn=0.000\,05$, and high nitrogen concentration. At $cn=0.000\,05$, the gap is located at the top of the Fermi energy, but inside the pure SWCNT conduction band. By increasing the nitrogen concentration, the low edge of the conduction band is moved and the gap is decreased.

For (20,0) and (40,), the gap is closed, hence a semiconductor to semimetal phase transition takes place. Also 1D van Hove singularities disappeared. But for the (10,0) zigzag SWCNT the gap is preserved and semimetal phase transition is not observed.

In the second case, we fixed the nitrogen concentration at $cn=0.1$, while varying the boron concentration. We found that E_g decreases with an increase in the boron concentration, and for (20,0), (40,0) at a critical concentration; it tended to zero. Figure 6 compares the average density of states for the low, $cb=0.000\,05$, and high boron concentrations. For the (20,0), (40,0) cases, the E_g is closed, similar to the first case, and the van Hove singularities also disappeared. Furthermore, the semiconductor to semimetal phase transition was also observed.

V. CONCLUSION

In conclusion, we have applied the EMSCA method to a disordered SWCNT in order to investigate the role of disorder in such materials. For a (10,10) armchair tube and also a zigzag (10,0) tube we found that the vacancies induce some bound states on their host neighbor sites, creating a band around the Fermi energy in the average density of states. The consequences of this band formation around the Fermi energy and also disappearance of the 1D van Hove singularities at high vacancy concentrations is that the density of states of an armchair and also a zigzag SWCNT become similar to a disordered (vacancy disorder) 2D graphene sheet density of states. A (10,0), (20,0), and (40,0) zigzag $B_{cb}N_{cn}C_{1-cb-cn}$ SWCNT alloy was investigated. We found that for a fixed boron (nitrogen) concentration, by increasing the nitrogen (boron) concentrations, the E_g decreases and for the cases of (20,0) and (40,0) at a critical concentration it becomes closed. Therefore, a semiconductor to a semimetal phase transition takes place. Our results show that we can control the E_g by changing the nitrogen (boron) concentration.

ACKNOWLEDGEMENT

The author would like to thank professor Rafii-Tabar for helpful discussion.

*Electronic address: rmoradian@razi.ac.ir

[1] R. Saito, G. Dresselhaus, and M. S. Dreesselhaus, Chem. Phys. Lett. **195**, 537 (1992).

[2] C. J. Brabec, A. Maiti, and J. Bernholc, Chem. Phys. Lett. **219**, 437 (1994).

[3] T. W. Ebbesen and T. Takada, Carbon **33**, 973 (1995).

[4] Y. Miyamoto, A. Rubio, M. L. Cohen, and S. G. Louie, Phys. Rev. B **50**, 4976 (1994); Y. Miyamoto, A. Rubio, S. G. Louie, and M. L. Cohen, *ibid.* **50**, 18 360 (1994); Y. Miyamoto, S. G. Louie, and M. L. Cohen, Phys. Rev. Lett. **76**, 2121 (1996); A. Rubio, Y. Miyamoto, X. Blase, M. L. Cohen, and S. G. Louie, Phys. Rev. B **53**, 4023 (1996).

[5] P. E. Lammert, V. H. Crespi, and A. Rubio, Phys. Rev. Lett. **87**, 136402 (2001).

[6] W. A. Harrison, *Electronic Structure and the Properties of the Solids* (W. H. Freeman and Co., San Francisco, 1980).

[7] T. Yoshioka, H. Suzuura, and T. Ando, J. Phys. Soc. Jpn. **72**, 2656 (2003).

[8] T. Kostyrko, M. Bartkowiak, and G. D. Mahan, Phys. Rev. B **59**, 3241 (1999).

[9] Hai-Feng Song, Jia-Lin Zhu, and Jia-Jiong Xiong, Phys. Rev. B **65**, 085408 (2002).
[10] X. Blase, J.-C. Charlier, A. De. Vita, and R. Car, Appl. Phys. Lett. **70**, 197 (1997).
[11] M. S. Ferreira, T. G. Dargam, R. B. Muniz, and A. Latge, Phys. Rev. B **62**, 16 040 (2000).
[12] Jin Choi, Yong-Hyun Kim, K. J. Chang, and David Tomanek, Phys. Rev. B **67**, 125421 (2003).
[13] Yi Liu and Hong Guo, Phys. Rev. B **69**, 115401 (2004).
[14] G. D. Mahan, Phys. Rev. B **69**, 125407 (2004).
[15] R. Moradian, B. L. Györffy, and J. F. Annett, Phys. Rev. Lett. **89**, 287002 (2002).
[16] Rostam Moradian, cond-mat/0405356 and cond-mat/0405357.
[17] R. Saito, M. Fujita, G. Dresselhaus, and M. S. Dreesselhaus, Phys. Rev. B **46**, 1804 (1991).